ACADEMIC PRESS

Available online at www.sciencedirect.com

SCIENCE DIRECT®

Journal of Sound and Vibration 266 (2003) 1053–1078

JOURNAL OF SOUND AND VIBRATION

www.elsevier.com/locate/jsvi

Phononic band gaps and vibrations in one- and two-dimensional mass–spring structures

J.S. Jensen*

Department of Mechanical Engineering, Section for Solid Mechanics, Technical University of Denmark Nils Koppels Allé, Building 404, DK-2800 Kgs. Lyngby, Denmark

Received 1 July 2002; accepted 1 October 2002

Abstract

The vibrational response of finite periodic lattice structures subjected to periodic loading is investigated. Special attention is devoted to the response in frequency ranges with gaps in the band structure for the corresponding infinite periodic lattice. The effects of boundaries, viscous damping, and imperfections are studied by analyzing two examples; a 1-D filter and a 2-D wave guide. In 1-D the structural response in the band gap is shown to be insensitive to damping and small imperfections. In 2-D the similar effect of damping is noted for one type of periodic structure, whereas for another type the band gap effect is nearly eliminated by damping. In both 1-D and 2-D it is demonstrated how the free structural boundaries affect the response in the band gap due to local resonances. Finally, 2-D wave guides are considered by replacing the periodic structure with a homogeneous structure in a straight and a 90° bent path, and it is shown how the vibrational response is confined to the paths in the band gap frequency ranges.

1. Introduction

In the last decade the interest in photonic band gap crystals has been great. Periodic structures of two materials with different di-electric properties may exhibit stop bands in the band structure where light waves cannot propagate—thus, photonic crystals can be constructed that effectively inhibit light at certain frequencies to be transmitted through them. Numerous research papers have appeared on the subject, see e.g., Refs. [1,2] and possible industrial applications have emerged such as e.g., wave guides, antennas, and lasers.

*Tel.: +45-45-25-4280; fax: +45-45-93-1475.
E-mail address: jsj@mek.dtu.dk (J.S. Jensen).

0022-460X/03/$ - see front matter
doi:10.1016/S0022-460X(02)01629-2

The work on photonic band gaps has led to a renewed interest in elastic wave propagation in periodic materials and especially the existence of the so-called phononic band gaps—i.e., stop bands in the band structure for propagation of elastic waves. However, the existence of frequency ranges where propagating wave solutions do not exist has already been demonstrated by Rayleigh [3]. Comprehensive reviews of earlier work on wave propagation and band gaps in periodic structures can be found in Refs. [4–6]. New research has focussed on theoretical predictions as well as experimental documentation of gaps in the band structure. Studies of periodic structures in one dimension include the experimental and theoretical analysis of string–mass chains [7], microtapered optical fibers [8], and theoretical work on band structures in locally periodic media governed by the wave equation [9]. In 2- and 3-D periodic structures gaps in the elastic band structure have been predicted using a variety of computational methods such as plane-wave expansion e.g., Refs. [10,11], finite elements (FEM) e.g., Refs. [12,13], the multiple scattering-theory (MST) e.g., Refs. [14,15], and a related Rayleigh method [16]. An extensive review of newer research in band structures of periodic materials can be found in Ref. [17], and frequently updated reference lists on phononic and photonic band gaps can be found at http://www.pbglink.com.

Unlike e.g., photonic crystals to the author's knowledge no direct applications of phononic band gap structures and materials have appeared. Little work has been published on analyzing the behavior of band gap materials in engineering structures, where the effects of the finite dimension, boundaries, damping, and imperfections must be addressed. Two recent exceptions are the studies of surface states and localization phenomena in periodic structures with defects [18,19]. It is the aim of this work to add knowledge that can be exploited in the development towards future applications. An extension of this work is the application of topology optimization techniques in the design of materials and structures with phononic band gaps [20,21].

In this work simple mass–spring models are used to demonstrate the dynamical behavior of periodic structures. The mass–spring models provide a convenient setting for the realization and visualization of periodic structures, for including damping and imperfections, and qualitatively they fully capture the phenomena involved. In Section 2 the mass–spring models of the *unit cells* are presented. The unit cells describe the repetitive units in the periodic structure. Band structures are calculated for the corresponding infinite lattices and for special cases approximate analytical frequency bounds for the gaps are obtained. Two examples are then provided in Section 3 in order to analyze the vibrational response of the periodic structures subjected to periodic loading in the band gap frequency ranges.

The first example deals with a 1-D structure with filtering properties (Section 3.2). Two different sizes of masses and springs are used in the structure, chosen so that it corresponds to a discrete model of aluminum and PMMA (acrylplastic) with filtering of longitudinal waves. It is shown how the response in the band gap frequency range depends on the number of unit cells in the structure and also how the response in the band gap is insensitive to moderate amounts of viscous damping and to small imperfections in the periodic structure.

The second example deals with a 2-D structure that can be utilized as a wave guide (Section 3.3). The structure is considered with two different types of unit cells, with masses and springs chosen to make the lattice correspond to a structure with a stiff aluminum inclusion in an epoxy matrix (type 1), or a heavy resonator of copper suspended in a flexible layer of silicone rubber in an epoxy matrix (type 2). With type 1 unit cells the response in the band gap depends only weakly on damping, whereas with type 2 unit cells damping almost eliminates the band gap effect. It is

shown for 2-D, as well as for the 1-D example, how the presence of boundaries creates local resonances that affect the response in the band gap. Finally, two wave guide structures are created by replacing the periodic structure with a homogeneous structure in a straight and in a 90° bent path. It is demonstrated how the vibrational response is confined to these paths when the frequency of the periodic loading is within the band gap.

2. Model: the unit cell—infinite lattices

The periodic structures to be considered are made up of a finite number of identical *unit cells*. These unit cells are the repetitive units that are used to describe the micro-structure (or material). If the unit cells are inhomogeneous, i.e., made up of different masses and/or springs, the corresponding structure is periodic, whereas with a homogeneous unit cell the structure is also homogeneous.

In the following, dispersion relations are obtained for wave propagation in infinite periodic lattices. Results are presented in form of band structures relating the frequency of the propagating waves to the wavenumber or wavevector.

2.1. The one-dimensional case—longitudinal waves

Fig. 1a shows the 1-D unit cell. Within the cell N masses m_j are connected by linear elastic springs with stiffness coefficients k_j. The small-amplitude displacement of the $(p+j)$th mass is governed by

$$m_j\ddot{u}_{p+j} = k_j(u_{p+j+1} - u_{p+j}) - k_{j-1}(u_{p+j} - u_{p+j-1}), \tag{1}$$

where p is an arbitrary integer.

Wave propagation through an infinite number of connected unit cells is considered and thus a travelling wave solution is assumed as

$$u_{p+j} = A_j e^{i((p+j)\gamma - \omega t)}, \tag{2}$$

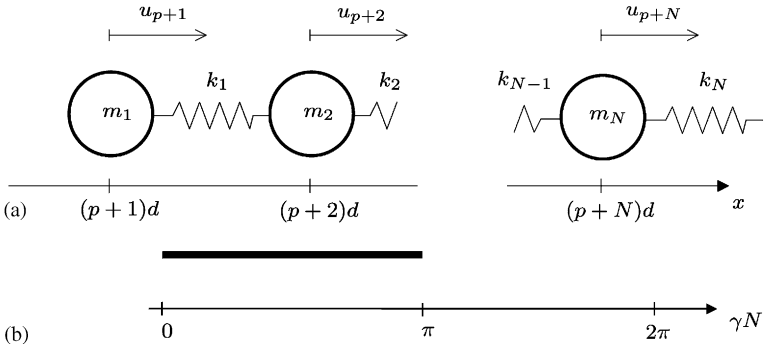

Fig. 1. (a) The 1-D unit cell with N masses m_j and springs k_j, and (b) the corresponding irreducible Brillouin zone indicating the range of the wavenumber γ evaluated when constructing the complete band structure from Eq. (8).

where A_j is the wave amplitude, γ the wavenumber, and ω is the wave frequency. Inserting Eq. (2) into Eq. (1) yields N linear complex equations

$$(\omega_j^2 - \omega^2)A_j = c_j^2 e^{i\gamma} A_{j+1} + (\omega_j^2 - c_j^2)e^{-i\gamma} A_{j-1}, \quad j = 1, \ldots, N, \tag{3}$$

where the following non-dimensional parameters have been introduced:

$$\omega_j^2 = \frac{k_j + k_{j-1}}{m_j}, \tag{4}$$

$$c_j^2 = \frac{k_j}{m_j}. \tag{5}$$

An infinite number of identical unit cells is considered and the following periodic boundary conditions can thus be applied:

$$A_{j-1} = A_N, \quad j = 1, \tag{6}$$

$$A_{j+1} = A_1, \quad j = N. \tag{7}$$

Eq. (3) forms with Eqs. (6) and (7) a standard complex eigenvalue problem

$$(\mathbf{S}(\gamma) - \omega^2 \mathbf{I})\mathbf{A} = \mathbf{0}, \tag{8}$$

that can be solved to construct the band structure of wave frequencies ω for known wavenumber γ.

It is not necessary to solve Eq. (8) for all values of γ. Due to the periodicity all propagating modes are captured by restricting the wavenumber to the irreducible Brillouin zone as shown in Fig. 1b [4]. The two end points in the zone, $\gamma N = 0$ and π, correspond to the masses in two neighboring unit cells moving in phase and in anti-phase, respectively.

2.1.1. Wave propagation for an inhomogeneous unit cell

As it is well known no gaps exist in the band structure for the homogeneous infinite lattice, i.e., waves of all frequencies are allowed to propagate. However, with an inhomogeneous unit cell gaps emerge in the band structure for the corresponding periodic infinite lattice. An example of an inhomogeneous unit cell is shown in Fig. 2a. This unit cell consists of four masses with the center masses and springs representing a material with lower stiffness to mass ratio (lower wave speed).

For the four-mass system ($N = 4$) the masses and springs are chosen as

$$m_1 = m_4 = 3.98 \text{ kg},$$

$$m_2 = m_3 = 1.69 \text{ kg},$$

$$k_1 = k_4 = 70.9 \times 10^9 \text{ kg/s}^2,$$

$$k_2 = k_3 = 5.28 \times 10^9 \text{ kg/s}^2 \tag{9}$$

which makes the mass–spring system correspond to a discrete model of a 0.15 m rod with the middle 50% of PMMA and the two ends of aluminum.[1]

[1] Material data: $E_{alu} = 70.9$ GPa, $\rho_{alu} = 2830$ kg/m^3, $E_{pmma} = 5.28$ GPa, $\rho_{pmma} = 1200$ kg/m^3.

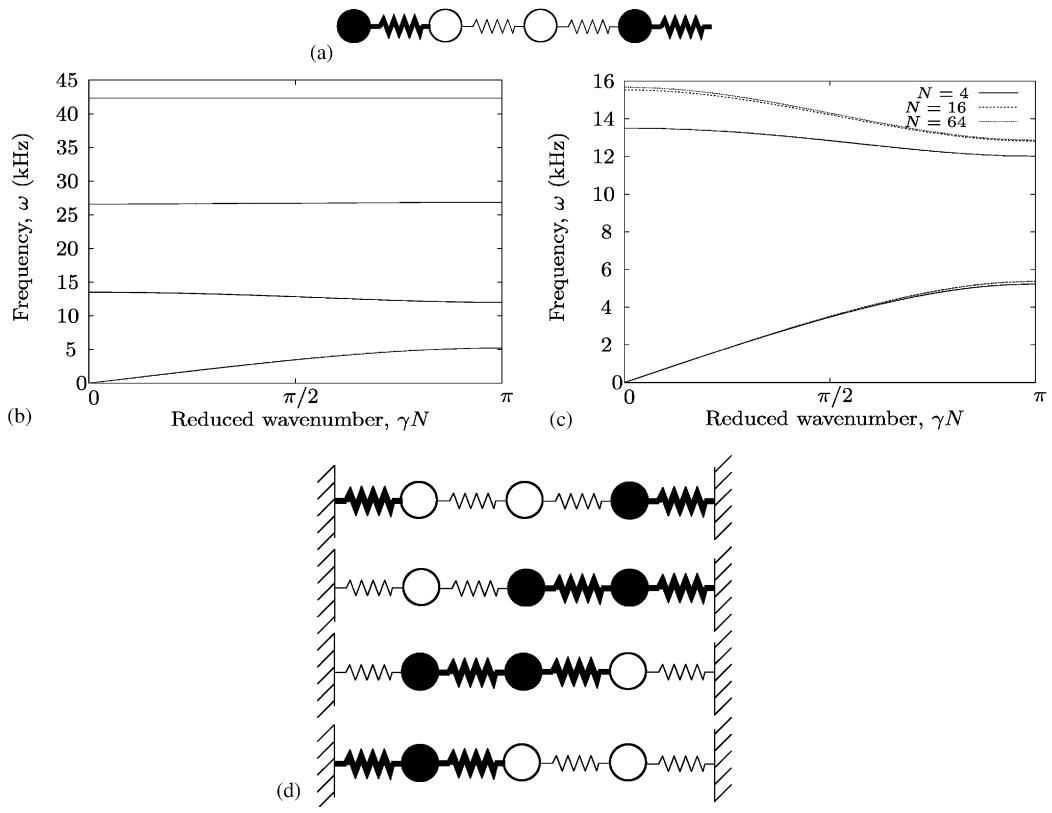

Fig. 2. (a) The unit cell with $N = 4$ (sizes of masses and springs given in the text), (b) band structure for wave propagation in the infinite periodic lattice, (c) close-up of the first gap including curves computed for $N = 16$ and 64, and (d) the four possible isolated systems with a single mass in the unit cells fixed.

As shown in Fig. 2b three large gaps appear in the band structure for $\omega \approx 5.2$–12.0, 13.5–26.6, and 26.8–42.3 kHz. In these frequency ranges no waves can propagate through the infinite periodic lattice. In Fig. 2c is shown a close-up of the lowest band gap including curves computed for higher values of N (a finer discretization of the unit cell with the middle $N/2$ masses and springs of PMMA). The band structure converges with increasing N towards the corresponding continuum model, but as appears the simple model with $N = 4$ gives a good estimation of the first band gap. For the other gaps the difference between the simple model and the continuum model is naturally larger.

The upper and lower frequency bounds for the first band gap can be accurately estimated by considering a simplified system (Fig. 2d). For wave propagation in the first pass band the four masses move in phase, corresponding to the fundamental mode of propagation. The first band gap appears when $\gamma N = \pi$ (Fig. 2a) for which the wave amplitude of one of the masses in the unit cells vanishes. Fig. 2d shows the four possible system configurations with a single mass in the unit cell fixed (replaced by a support in the figure). It is now possible to estimate the lower and upper frequency bound of the band gap by identifying the lowest and highest fundamental eigenfrequency for the four configurations. The system third from top in Fig. 2d has the lowest

fundamental eigenfrequency $\omega = 5.2$ kHz which matches the lower band gap frequency well, and the system at the top has the highest fundamental eigenfrequency found as $\omega = 12.0$ kHz giving a good estimation of the upper band gap frequency.

In the band gaps, instead of propagating modes, solutions exist for purely imaginary wavenumbers. Introducing the imaginary wavenumber $\gamma \to \mathrm{i}\gamma$ into the solution form (2) yields

$$u_{p+j} = A_j \mathrm{e}^{-(p+j)\gamma} \mathrm{e}^{-\mathrm{i}\omega t} \tag{10}$$

showing that the solution is a standing wave with an amplitude of vibration that is exponentially decaying spatially.

2.2. The 2-D case—in-plane elastic waves

A 2-D unit cell is shown in Fig. 3a. Within the cell $N \times N$ masses are arranged in a square configuration with each mass connected to eight neighboring masses with springs. The four springs connected to the j,kth mass in the 0°, 45°, 90°, and 135° directions from the x-axis are denoted $k_{j,k,1}$, $k_{j,k,2}$, $k_{j,k,3}$, and $k_{j,k,4}$.

The equations of motion governing the small-amplitude displacements of the $(p+j),(q+k)$th mass in the x and y directions (u, v) are given as:

$$\begin{aligned} m_{j,k}\ddot{u}_{p+j,q+k} = {} & k_{j,k,1}(u_{p+j+1,q+k} - u_{p+j,q+k}) \\ & + \tfrac{1}{2}k_{j,k,2}(u_{p+j+1,q+k+1} - u_{p+j,q+k} + v_{p+j+1,q+k+1} - v_{p+j,q+k}) \\ & + \tfrac{1}{2}k_{j,k,4}(u_{p+j-1,q+k+1} - u_{p+j,q+k} - v_{p+j-1,q+k+1} + v_{p+j,q+k}) \\ & + k_{j-1,k,1}(u_{p+j-1,q+k} - u_{p+j,q+k}) \\ & + \tfrac{1}{2}k_{j-1,k-1,2}(u_{p+j-1,q+k-1} - u_{p+j,q+k} + v_{p+j-1,q+k-1} - v_{p+j,q+k}) \\ & + \tfrac{1}{2}k_{j+1,k-1,4}(u_{p+j+1,q+k-1} - u_{p+j,q+k} - v_{p+j+1,q+k-1} + v_{p+j,q+k}), \end{aligned} \tag{11}$$

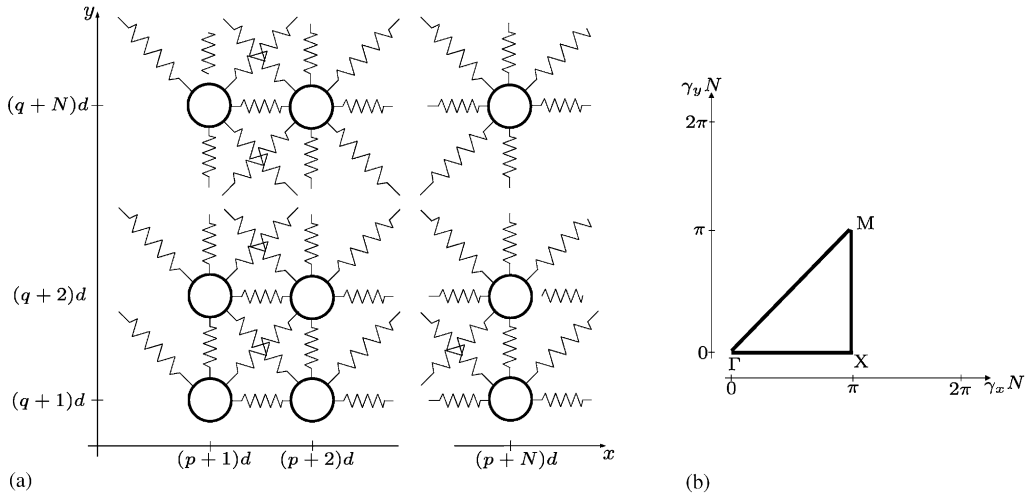

Fig. 3. (a) The 2-D square unit cell with $N \times N$ masses and corresponding $4 \times N \times N$ springs, and (b) the corresponding irreducible Brillouin zone indicating the triangular path on which the wavevector γ should be evaluated in Eq. (21).

$$\begin{aligned} m_{j,k}\ddot{v}_{p+j,q+k} = {} & k_{j,k,3}(v_{p+j,q+k+1} - v_{p+j,q+k}) \\ & + \tfrac{1}{2}k_{j,k,2}(v_{p+j+1,q+k+1} - v_{p+j,q+k} + u_{p+j+1,q+k+1} - u_{p+j,q+k}) \\ & + \tfrac{1}{2}k_{j,k,4}(v_{p+j-1,q+k+1} - v_{p+j,q+k} - u_{p+j-1,q+k+1} + u_{p+j,q+k}) \\ & + k_{j,k-1,3}(v_{p+j,q+k-1} - v_{p+j,q+k}) \\ & + \tfrac{1}{2}k_{j-1,k-1,2}(v_{p+j-1,q+k-1} - v_{p+j,q+k} + u_{p+j-1,q+k-1} - u_{p+j,q+k}) \\ & + \tfrac{1}{2}k_{j+1,k-1,4}(v_{p+j+1,q+k-1} - v_{p+j,q+k} - u_{p+j+1,q+k-1} + u_{p+j,q+k}), \end{aligned} \tag{12}$$

where p and q are arbitrary.

As in the 1-D case a travelling wave solution is assumed in the infinite lattice

$$u_{p+j,q+k} = A_{j,k}\mathrm{e}^{\mathrm{i}((p+j)\gamma_x+(q+k)\gamma_y-\omega t)}, \tag{13}$$

$$v_{p+j,q+k} = B_{j,k}\mathrm{e}^{\mathrm{i}((p+j)\gamma_x+(q+k)\gamma_y-\omega t)}, \tag{14}$$

where $A_{j,k}$ and $B_{j,k}$ are the wave amplitudes, ω the wave frequency, and γ_x and γ_y are the two components of the wavevector $\boldsymbol{\gamma}$.

With the following non-dimensional constants defined:

$$\omega_{x,j,k}^2 = \frac{k_{j,k,1} + k_{j-1,k,1} + \frac{1}{2}(k_{j,k,2} + k_{j,k,4} + k_{j-1,k-1,2} + k_{j+1,k-1,4})}{m_{j,k}}, \tag{15}$$

$$\omega_{y,j,k}^2 = \frac{k_{j,k,3} + k_{j,k-1,3} + \frac{1}{2}(k_{j,k,2} + k_{j,k,4} + k_{j-1,k-1,2} + k_{j+1,k-1,4})}{m_{j,k}}, \tag{16}$$

$$\tilde{k}_{j,k} = \frac{\frac{1}{2}(k_{j,k,2} - k_{j,k,4} + k_{j-1,k-1,2} - k_{j+1,k-1,4})}{m_{j,k}}, \tag{17}$$

$$c_{j,k}^2 = \frac{k_{j,k}}{m_{j,k}}, \tag{18}$$

Eqs. (11) and (12) become

$$\begin{aligned} (\omega_{x,j,k}^2 - \omega^2)A_{j,k} + \tilde{k}_{j,k}B_{j,k} = {} & c_{j,k,1}^2\mathrm{e}^{\mathrm{i}\gamma_x}A_{j+1,k} \\ & + \tfrac{1}{2}c_{j,k,2}^2(\mathrm{e}^{\mathrm{i}(\gamma_x+\gamma_y)}A_{j+1,k+1} + \mathrm{e}^{\mathrm{i}(\gamma_x+\gamma_y)}B_{j+1,k+1}) \\ & + \tfrac{1}{2}c_{j,k,4}^2(\mathrm{e}^{\mathrm{i}(\gamma_y-\gamma_x)}A_{j-1,k+1} - \mathrm{e}^{\mathrm{i}(\gamma_y-\gamma_x)}B_{j-1,k+1}) \\ & + c_{j-1,k,1}^2\mathrm{e}^{-\mathrm{i}\gamma_x}A_{j-1,k} \\ & + \tfrac{1}{2}c_{j-1,k-1,2}^2(\mathrm{e}^{-\mathrm{i}(\gamma_x+\gamma_y)}A_{j-1,k-1} + \mathrm{e}^{-\mathrm{i}(\gamma_x+\gamma_y)}B_{j-1,k-1}) \\ & + \tfrac{1}{2}c_{j+1,k-1,4}^2(\mathrm{e}^{\mathrm{i}(\gamma_x-\gamma_y)}A_{j+1,k-1} - \mathrm{e}^{\mathrm{i}(\gamma_x-\gamma_y)}B_{j+1,k-1}), \end{aligned} \tag{19}$$

$$
\begin{aligned}
(\omega_{y,j,k}^2 - \omega^2)B_{j,k} + \tilde{k}_{j,k}A_{j,k} = {} & c_{j,k,3}^2 e^{i\gamma_y} B_{j,k+1} \\
& + \tfrac{1}{2} c_{j,k,2}^2 (e^{i(\gamma_x+\gamma_y)} B_{j+1,k+1} + e^{i(\gamma_x+\gamma_y)} A_{j+1,k+1}) \\
& + \tfrac{1}{2} c_{j,k,4}^2 (e^{i(\gamma_y-\gamma_x)} B_{j-1,k+1} - e^{i(\gamma_y-\gamma_x)} A_{j-1,k+1}) \\
& + c_{j,k-1,3}^2 e^{-i\gamma_y} B_{j-1,k} \\
& + \tfrac{1}{2} c_{j-1,k-1,2}^2 (e^{-i(\gamma_x+\gamma_y)} B_{j-1,k-1} + e^{-i(\gamma_x+\gamma_y)}) A_{j-1,k-1} \\
& + \tfrac{1}{2} c_{j+1,k-1,4}^2 (e^{i(\gamma_x-\gamma_y)} B_{j+1,k-1} - e^{i(\gamma_x-\gamma_y)} A_{j+1,k-1})
\end{aligned} \tag{20}
$$

with periodic boundary conditions applied using a 2-D equivalent of Eqs. (6) and (7).

The corresponding eigenvalue problem is set up

$$
(\mathbf{S}(\gamma_x, \gamma_y) - \omega^2 \mathbf{I})\mathbf{A} = \mathbf{0} \tag{21}
$$

and solved for the wave frequency ω for known wavevector components γ_x and γ_y. As in the 1-D case it is not necessary to analyze Eq. (21) for all γ_x and γ_y. In Fig. 3b the irreducible Brillouin zone in two dimensions is shown, [4], where the analysis can be restricted to the triangular zone if the unit cell is square and symmetrical. Furthermore, it is only necessary to search the zone on the exterior boundary, i.e., along the path $\Gamma - \mathrm{X} - \mathrm{M} - \Gamma$, since the extremums of the wave frequencies are always found on the zone boundary.[2]

2.2.1. *Band gaps for a stiff inclusion: type 1 unit cell*

The homogeneous unit cell produces a band structure without gaps, as was also the case for the 1-D problem.

A unit cell with a band gap is shown in Fig. 4a with the corresponding band structure shown in Fig. 4b. A cell with 5×5 masses and connecting springs is chosen where the center 3×3 masses and corresponding springs represent a heavy and stiff inclusion and the remaining masses and springs are the lighter and more flexible matrix material.

The values of masses and springs are

$$
m_{mat} = 1.82 \times 10^{-2} \text{ kg},
$$

$$
m_{inc} = 4.53 \times 10^{-2} \text{ kg},
$$

$$
k_{mat,1} = k_{mat,3} = 2 \times k_{mat,2} = 2 \times k_{mat,4} = 4.10 \times 10^9 \text{ kg/s}^2,
$$

$$
k_{inc,1} = k_{inc,3} = 2 \times k_{inc,2} = 2 \times k_{inc,4} = 70.9 \times 10^9 \text{ kg/s}^2. \tag{22}
$$

The values in Eq. (22) are chosen so that the model corresponds to a 0.02 m $\times$ 0.02 m unit cell of epoxy matrix with an aluminum inclusion. By choosing the springs $k_{,2}$, and $k_{,4}$ to be half the size of the springs $k_{,1}$, and $k_{,3}$, as in Eq. (22), a good qualitative agreement is obtained between the mass–spring model and a plane-strain 2-D continuum model of materials with the Poisson ratio near $\nu = 0.3$.

[2] To the author's knowledge no proof of this has been published. However, it appears to be generally accepted and in the numerical examples presented in this paper this is indeed so.

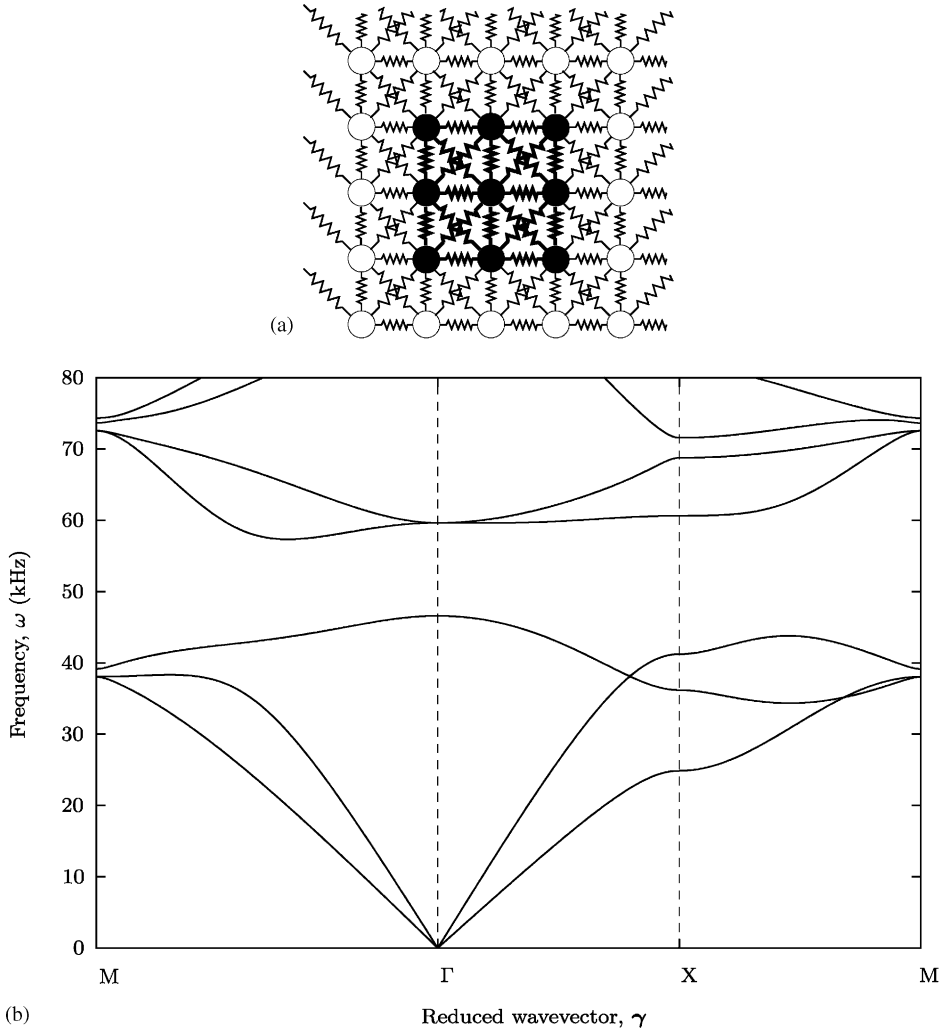

Fig. 4. (a) The 5×5 mass–spring unit cell (denoted type 1) modelling a stiff inclusion (center 3×3 masses and springs) in a surrounding matrix, and (b) the corresponding band structure for wave propagation in the infinite periodic lattice structure.

As appears from Fig. 4b a gap appears in the band structure for $\omega \approx 46.6$–57.3 kHz between the third and fourth bands. In this frequency range waves cannot propagate in the infinite lattice regardless of the direction of propagation. The band gap calculated for this mass-spring unit cell model corresponds qualitatively to the band gap found for the corresponding continuum model, see e.g., Refs. [15,20].

2.2.2. *Band gaps for a heavy resonator: type 2 unit cell*

Alternatively, band gaps can be obtained in the lower frequency range by placing a heavy inclusion in soft suspension with a surrounding matrix material. The heavy inclusion acts as a

local resonator and splits up the band structure. Recently, band gaps for such structures were demonstrated in Refs. [14,22], with the former pointing out a possible application in noise reduction due to the low band gap frequency range.

Fig. 5a shows the unit cell and the corresponding band structure is shown in Fig. 5b. The masses and springs in the model have been chosen as

$$m_{mat} = 1.27 \times 10^{-2} \text{ kg},$$

$$m_{inc} = 9.93 \times 10^{-2} \text{ kg},$$

$$k_{mat,1} = k_{mat,3} = 2 \times k_{mat,2} = 2 \times k_{mat,4} = 4.10 \times 10^{9} \text{ kg/s}^2,$$

$$k_{inc,1} = k_{inc,3} = 2 \times k_{inc,2} = 2 \times k_{inc,4} = 118 \times 10^{9} \text{ kg/s}^2,$$

$$k_{susp,1} = k_{susp,3} = 2 \times k_{susp,2} = 2 \times k_{susp,4} = 4.00 \times 10^{6} \text{ kg/s}^2. \tag{23}$$

With the parameters in Eq. (23) the model corresponds to a 0.02 m × 0.02 m unit cell of an epoxy matrix with a copper inclusion suspended in a thin massless layer of silicone rubber.[3]

The band gap frequency range can be accurately predicted. The local resonance of the heavy inclusion in the soft suspension splits up the band structure and determines the lower bound for the band gap

$$\omega_1 \approx \sqrt{\frac{K_{susp}}{M_{inc}}} = \sqrt{\frac{7k_{susp}}{4m_{inc}}} \approx 1.34 \text{ kHz}. \tag{24}$$

The first possible propagation mode above the band gap is when the inclusion and the matrix material can move essentially rigidly in anti-phase. With the matrix motion denoted x and the motion of the inclusion y, the rigid motion is governed by the 2-d.o.f. system

$$M_{mat}\ddot{x} = K_{susp}(y - x), \tag{25}$$

$$M_{inc}\ddot{y} = K_{susp}(x - y), \tag{26}$$

that yields the upper bound frequency

$$\omega_2 \approx \sqrt{\frac{K_{susp}(M_{inc} + M_{mat})}{M_{inc}M_{mat}}} = \sqrt{\frac{7k_{susp}(4m_{inc} + 32m_{mat})}{4m_{inc}32m_{mat}}} \approx 1.88 \text{ kHz} \tag{27}$$

as well as the ratio of amplitudes at the upper frequency bound

$$\frac{y}{x} = 1 - \omega_2^2 \frac{M_{mat}}{K_{susp}} = -\frac{M_{mat}}{M_{inc}} = -\frac{32m_{mat}}{4m_{inc}} \approx -1.02. \tag{28}$$

It is noted that the frequency bounds in Eqs. (24) and (27) correspond well to the gap frequencies shown in the inset in Fig. 5b.

[3] Material data: $E_{epo} = 4.1$ GPa, $\rho_{epo} = 1140$ kg/m^3, $E_{cop} = 118$ GPa, $\rho_{cop} = 8940$ kg/m^3, $E_{rub} = 4$ MPa.

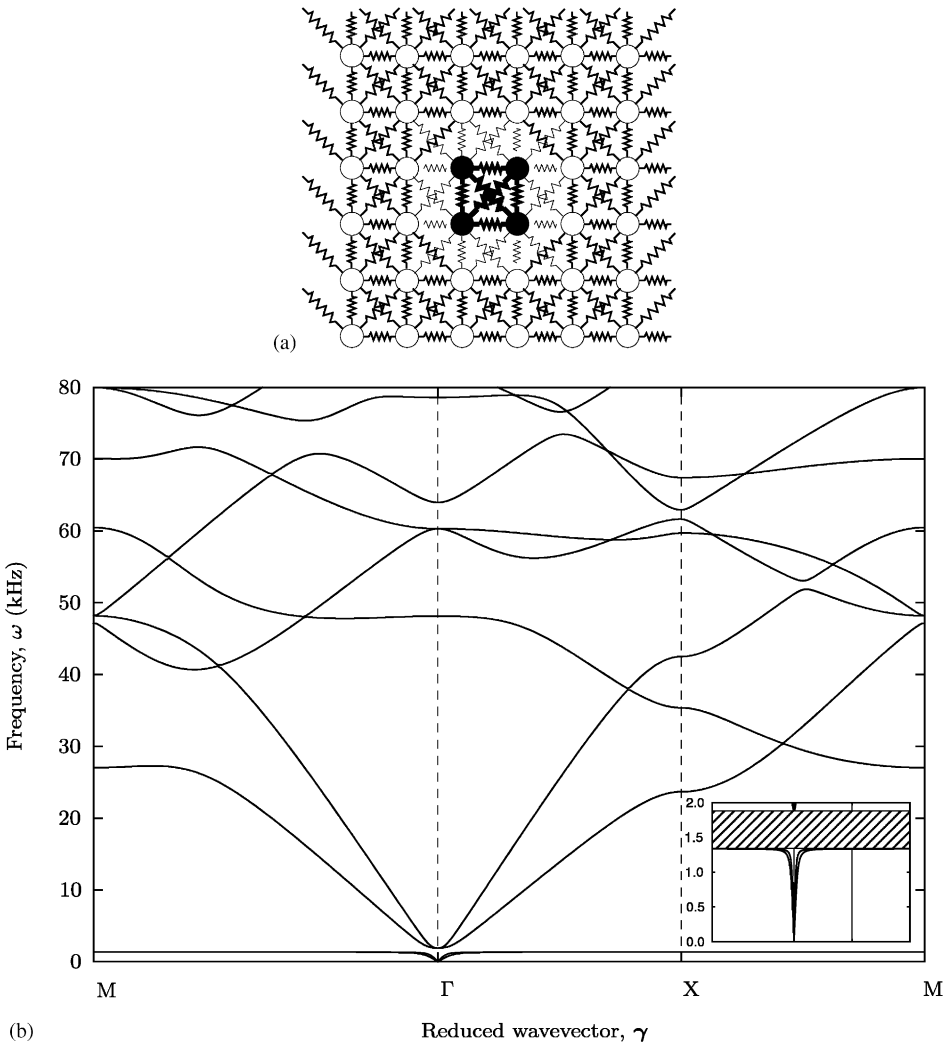

Fig. 5. (a) The 6×6 mass–spring unit cell (denoted type 2) modelling a heavy stiff resonator (center 2×2 masses and springs) in soft suspension (surrounding springs) connected to a surrounding matrix, and (b) the corresponding band structure for wave propagation in the infinite periodic lattice. The inset shows a magnification of the band structure from $\omega = 0$–2 kHz with the band gap shown hatched.

3. Finite lattice structures

Wave propagation in infinite, undamped, periodic lattices was analyzed in Section 2. In this section the behavior of finite periodic structures subjected to periodic loading is considered in order to study the effects of boundaries, damping, and imperfections in the periodic structure.

The finite structures are treated by two examples: A 1-D-periodic structure that acts as a filter and a 2-D-periodic structure that can be used to guide waves.

3.1. Model equations

A finite number of 1-D or 2-D unit cells are considered. The displacement vector $\mathbf{u}(t) = \{u_1 u_2 \ldots u_{N_{tot}}\}^{\mathrm{T}}$ is introduced where N_{tot} is the total number of degrees of freedom in the model. In 1-D the vector takes the form: $\mathbf{u}(t) = \{u_1 \ldots u_N u_{N+1} \ldots u_{MN}\}^{\mathrm{T}}$, where M is the number of unit cells. In 2-D the vector is given as $\mathbf{u}(t) = \{u_{1,1} v_{1,1} \ldots u_{1,M_y N} v_{1,M_y N} \ldots u_{M_x N, M_y N} v_{M_x N, M_y N}\}^{\mathrm{T}}$, where M_x and M_y is the number of unit cells in the x and y directions, respectively.

The model equations that govern the small-amplitude displacement of the masses can now be taken directly from Eq. (1) or (11)–(12) and written as

$$\mathbf{M}\ddot{\mathbf{u}} + \mathbf{C}\dot{\mathbf{u}} + \mathbf{K}\mathbf{u} = \mathbf{f}e^{i\Omega t}, \tag{29}$$

where $\mathbf{M}$ and $\mathbf{K}$ is the assembled mass- and stiffness-matrices, respectively, $\mathbf{C}$ is an added viscous damping matrix, and $\mathbf{f}$ is a vector of forces of frequency Ω.

A diagonal damping matrix is used to model the viscous damping with the components c_i expressed in terms of the actual to critical damping ratio ζ_i from the relation

$$\zeta_i = \frac{c_i}{2\sqrt{m_i \bar{k}_i}}, \tag{30}$$

where m_i is the mass corresponding to the ith dof and $\bar{k}_i$ is an equivalent stiffness defined as $m_i\omega_i^2$, cf. Eq. (4) in 1-D and Eqs. (15) and (16) in 2-D.

With the time dependency of the displacement vector

$$\mathbf{u}(t) = \mathbf{a}e^{i\Omega t} \tag{31}$$

inserted into Eq. (29), the linear set of equations to be solved for the amplitudes $\mathbf{a}$ is given as

$$(-\Omega^2\mathbf{M} + i\Omega\mathbf{C} + \mathbf{K})\mathbf{a} = \mathbf{f}. \tag{32}$$

3.2. Example 1: a 1-D filter

An application for band gaps in a 1-D lattice is as pass- or stop-band filters. In theory, for an infinite, and perfectly periodic lattice without damping, perfect filtering properties exist with alternating pass bands and complete stop bands. The properties of finite lattice structures subjected to periodic loading is here considered by analyzing the effect of the number of unit cells in the structure, viscous damping, and imperfections in the periodic structure.

The unit cell considered in Section 2.1 with four masses and springs is used to describe the periodic structure. As previously stated, this can be seen as a discrete model of a 0.15 m unit cell consisting of 50% aluminum and 50% PMMA. In Section 2.1 it was shown that for the infinite lattice this unit cell displays a band gap between approximately 5.2–12 kHz. Another band gap appears above 13.5 kHz but the focus is here put on the response in the first gap.

Fig. 6a shows the model of the structure with M unit cells. The structure is subjected to a periodic loading $f\cos\Omega t$ at the left end. Fig. 6b shows the corresponding computational mass–spring model with 10 unit cells ($M = 10$) and the four mass unit cell ($N = 4$).

In the following sections, the filtering properties of this structure are analyzed for different choice of system parameters. The response of the structure is typically given for the last mass in the lattice and presented as frequency response functions (FRF) showing the acceleration of the

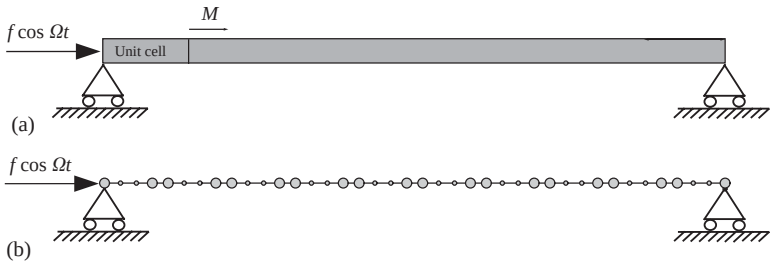

Fig. 6. (a) Structure made of M unit cells with a periodic loading $f\cos\Omega t$ acting in one end, and (b) the corresponding computational mass–spring model with $M = 10$ and the unit cell with 4 masses ($N = 4$).

mass for a reference force amplitude. The FRF curves are computed by solving the full set of linear equations (32) for each frequency Ω.

3.2.1. The number of unit cells

An important parameter in the performance of the filter is of course the number of unit cells used. If only a few unit cells are used the potential attenuation of the signal in the band gap frequency range is lower than if more unit cells are used.

Fig. 7a displays the FRF for the last mass in the lattice structure when it is subjected to a periodic loading of the first mass. Curves are shown for $M = 2, 5, 10$, and for comparison the band gap boundaries calculated for the infinite lattice are shown with vertical dashed lines.

For $M = 2$ the band gap is detectable from the curve but the drop in response inside the band gap is not much larger than the response drops between other resonance frequencies. With more unit cells included the gap clearly appears—resonances are clustered outside the gap, the response is reduced significantly inside the gap, and the steepness of curves increases at the band gap boundaries. With even more unit cells included the steepness of the response curves near these boundaries can, in principle, be as large as desired.

When M is large the computed band gap boundaries for the infinite lattice are seen to correspond well with the band gap detectable from the FRF. However, a small discrepancy is noted near the first gap $\Omega \approx 5.3$ kHz where resonance peaks appear just inside the gap boundary. The resonance here is associated with a local eigenmode located near the boundary of the structure where the boundary conditions are different.

This boundary effect is displayed in Fig. 7b. Here, the response of all masses in the structure is shown for four frequencies. The short-dashed line for $\Omega = 5.27$ kHz corresponds to the boundary mode frequency. The two curves for frequencies inside the band gap (i.e., $\Omega = 5.27$ and 6.00 kHz) display an exponentially decreasing amplitude away from the point of excitation as predicted from Eq. (10), but the boundary mode is seen as an increase in the response towards the end of the structure. The curves for the two other frequencies outside the band gap correspond to excitation of a low and a high vibration mode.

3.2.2. Viscous damping and imperfections

Fig. 8a shows FRF-curves for the considered structure with $M = 10$ without damping and with three different amounts of viscous damping characterized by the damping ratios $\zeta = 0.1\%$, 1.0%, and 5.0% added.

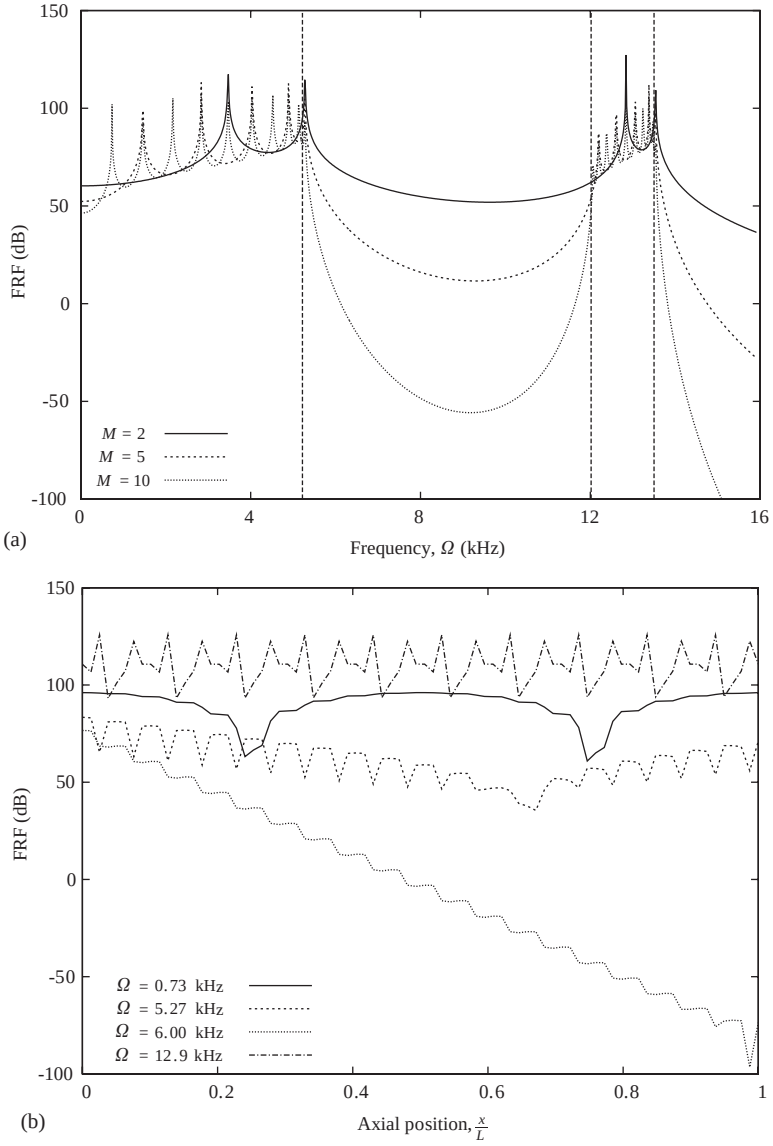

Fig. 7. (a) FRF-curves for the last mass in the lattice for different numbers of unit cells in the structure. Vertical dashed lines indicate the band gap boundaries calculated for the infinite periodic structure, and (b) the response for all masses for $M = 10$ for four different frequencies.

For low values of damping the response resembles that of the undamped structure, except that the peaks at resonance are reduced, i.e., a normal effect of added damping. In the band gap the responses are hardly changed by small amounts of damping. Only with strong damping added ($\zeta = 5\%$) is the response inside the gap affected.

Like with damping it can be expected that some imperfection in the periodic structure is present. Fig. 8b shows the effect of adding some level of disorder to the perfect periodic structure.

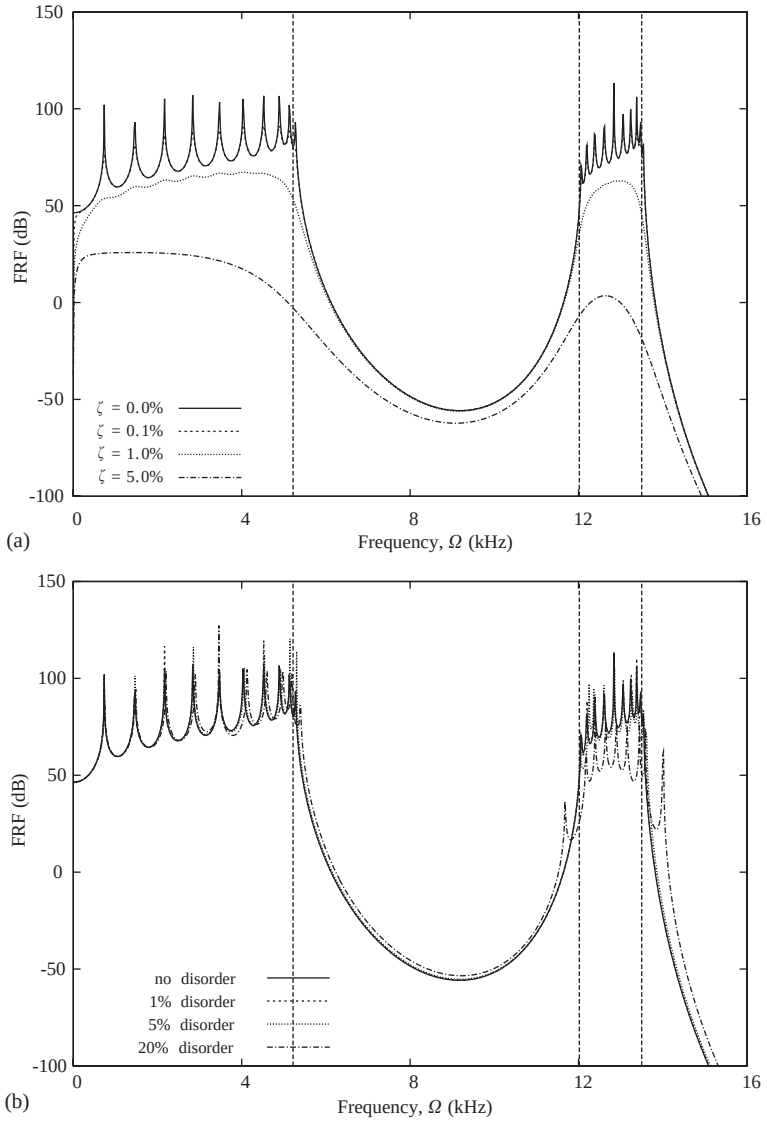

Fig. 8. (a) The influence on the response of the last mass of added viscous damping characterized by the actual to critical damping ratio ζ of the individual masses, and (b) the influence of random disorder of the sizes of the individual masses. For all curves $M = 10$.

The imperfections are simulated by adding a random variation to each mass size. The variation is indicated by a disorder percentage representing the maximum variation of the mass relative to its nominal value.

Fig. 8b shows that the response is insensitive to the presence of small imperfections. Only if the structure deviates significantly from the perfect periodic (20% disorder) is the response inside the band gap noticeably changed by e.g., the presence of local resonances. But even with this high level of imperfection the band gap is still clearly seen in the response.

3.3. Example 2: a 2-D waveguide

In Sections 2.2.1 and 2.2.2 it was shown how two different inhomogeneous unit cells have gaps in the band structure for 2-D in-plane waves. In this section the vibrational response of periodic structures with these two types of unit cells are analyzed when it is subjected to periodic loading. The effects of the number of unit cells, viscous damping, and boundary effects are considered and it is shown also how a structure with band gap unit cells can act as a wave guide.

Fig. 9a displays a model of the structure composed of a number of unit cells, M_x in one direction and M_y in the other. A periodic loading $f\cos\Omega t$ is applied centrally on the upper boundary and the structure is simply supported at the two lower corners. Fig. 9b shows the corresponding computational mass–spring model for $M_x = M_y = 7$ with type 1 unit cell.

3.3.1. Type 1 unit cells

Fig. 10 shows FRF-curves for the structure with type 1 unit cells (5×5 masses corresponding to a 0.02 m $\times$ 0.02 m epoxy matrix with a square aluminum inclusion). Indicated in the figure with vertical dashed lines are the band gap boundaries for the infinite periodic lattice, as seen in Fig. 5. Fig. 10a shows the response in the bottom of the structure (point A in Fig. 9a), and Fig. 10b on the side of the structure (point B). For $M_x = M_y = 3$ the band gap is not clearly detectable from the response, with e.g., several resonance peaks appearing inside the band gap boundaries. With more unit cells the response clearly drops inside the gap. However for all curves resonance peaks and a high response are seen from $\Omega \approx 55$ kHz and up to the upper boundary frequency. These resonance peaks are associated with local resonances for the boundary elements, as in the 1-D case.

Fig. 11 shows contour plots of the response in the structure for two frequencies. The response in Fig. 11a is calculated for $\Omega = 52.1$ kHz, corresponding to a point in the middle of the band gap and shows clearly how the response is localized near the point of excitation. For $\Omega = 54.8$ kHz a high response is seen to be localized near the boundary of the structure. This frequency is inside the band gap range but appears as waves can still propagate along the boundary elements.

3.3.2. Type 2 unit cells

The type 2 unit cell also displays a band gap, but in a lower frequency range than type 1 unit cell. This unit cell corresponds to a 0.02 m $\times$ 0.02 m epoxy matrix with a copper inclusion in a soft suspension of silicon rubber.

Fig. 12 shows the FRF-curves and the corresponding band gap frequency range in points A and B. As expected, the response drops inside the band gap, but a significant reduction is seen only very locally near the lower band gap frequency boundary, i.e. the local resonance frequency of the inclusions.

A contour plot of the response for $\Omega = 1.34$ kHz is shown in Fig. 13a, the frequency where the response drops to a minimum. The vibrations are seen to be localized near the point of excitation with the inclusions vibrating with a higher amplitude than the surrounding masses throughout the whole structure.

Fig. 13b shows the response for $\Omega = 1.90$ kHz, i.e., slightly above the upper band gap frequency. Here, the response is seen to be nearly constant over most of the domain except near

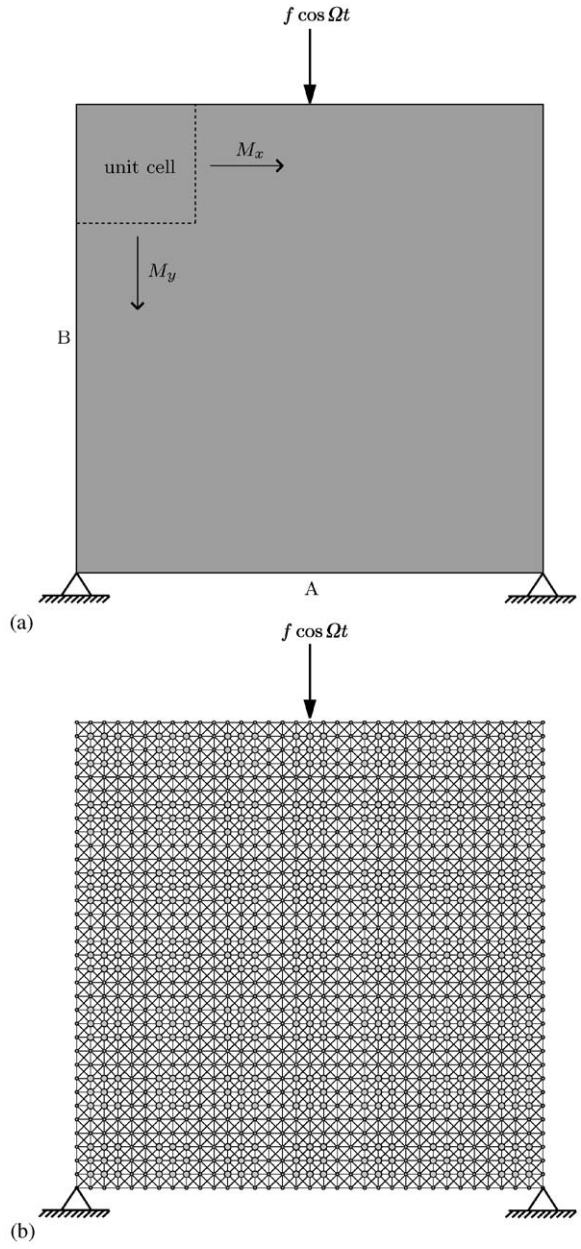

Fig. 9. (a) The structure with $M_x \times M_y$ unit cells with a periodic loading $f\cos\Omega t$ acting centrally at the top boundary and simple supports at the bottom corners, and (b) the corresponding computational model for $M_x = M_y = 7$ and type 1 unit cells.

the supports. This corresponds well to the motion predicted by Eq. (28), where the inclusions and the matrix material are predicted to move essentially rigidly in anti-phase with nearly identical amplitudes.

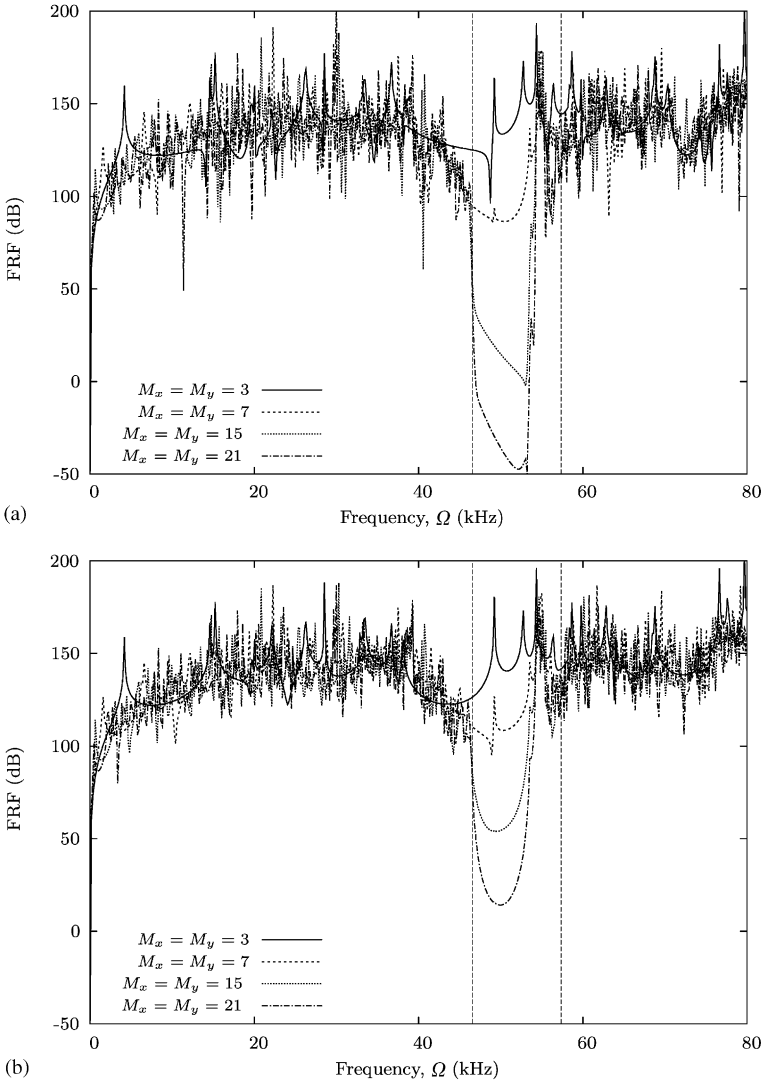

Fig. 10. The structural response with $M_x \times M_y$ type 1 unit cells included in the structure, (a) shows the response in point A and (b) in point B.

3.3.3. *Viscous damping*

Fig. 14a shows the effect of adding damping to the structure with $M_x = M_y = 21$ and type 1 unit cells. The undamped FRF curve is shown for comparison together with curves for damping ratios of $\zeta = 0.1\%$ and 1.0%. Fig. 14b shows the corresponding curves with type 2 unit cells.

Clearly, with type 1 unit cells the band gap is still noticeable with damping present, even when the damping is so strong that all resonance peaks have nearly disappeared from the response. However, with type 2 unit cells in the structure the band gap practically disappears for strong

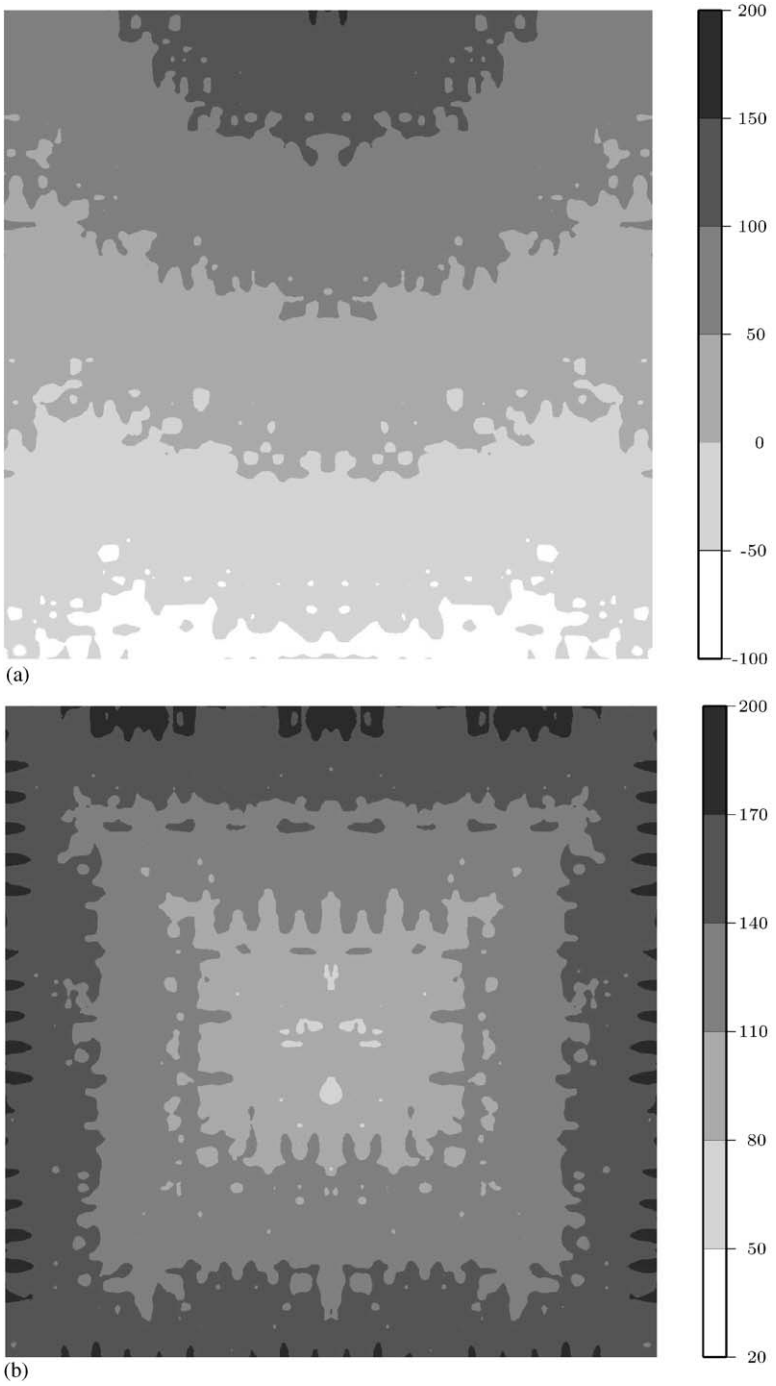

Fig. 11. (a) Contour plot of the structural response (in dB) for $\Omega = 52.1$ kHz, and (b) for $\Omega = 54.8$ kHz. Type 1 unit cells with $M_x = M_y = 21$.

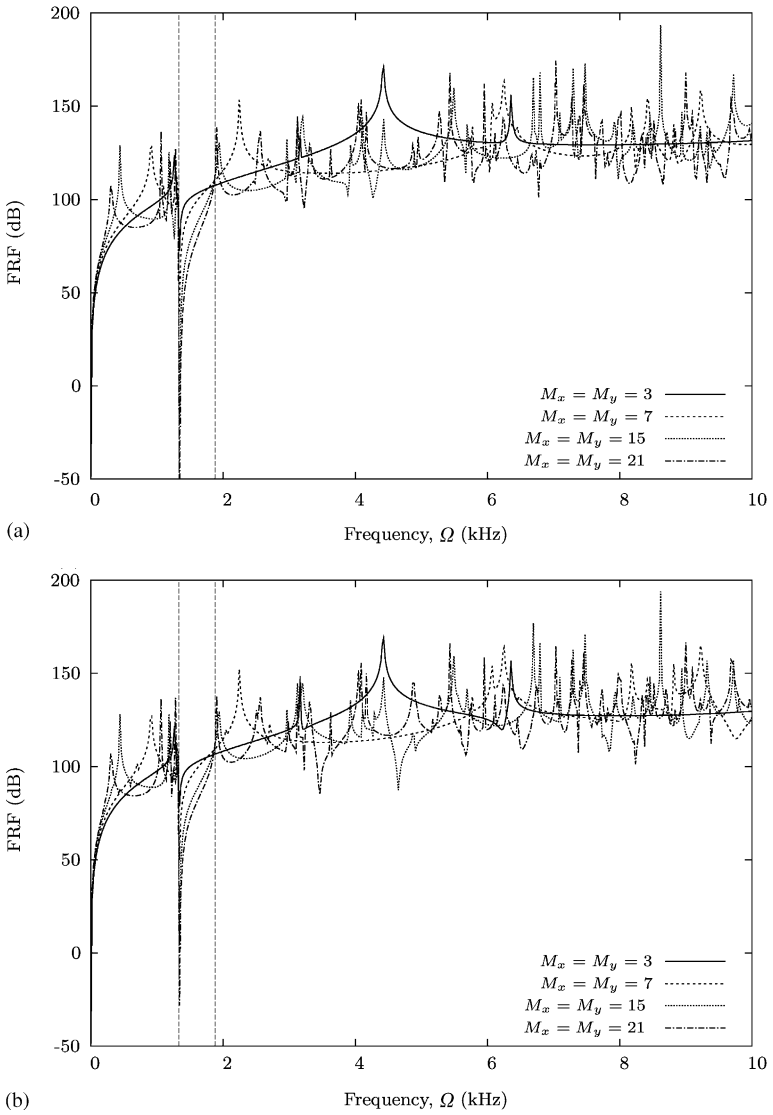

Fig. 12. The structural response with $M_x \times M_y$ type 2 unit cells included in the structure, (a) shows the response in point A and (b) in point B.

damping, and although for $\zeta = 0.1\%$ a drop in the response is noticed near the gap it is hardly distinguishable from other response drops between resonances.

3.3.4. *Wave guides*

It has been demonstrated how structures assembled from unit cells with band gaps may exhibit a large reduction in the structural response away from the point of excitation when subjected to

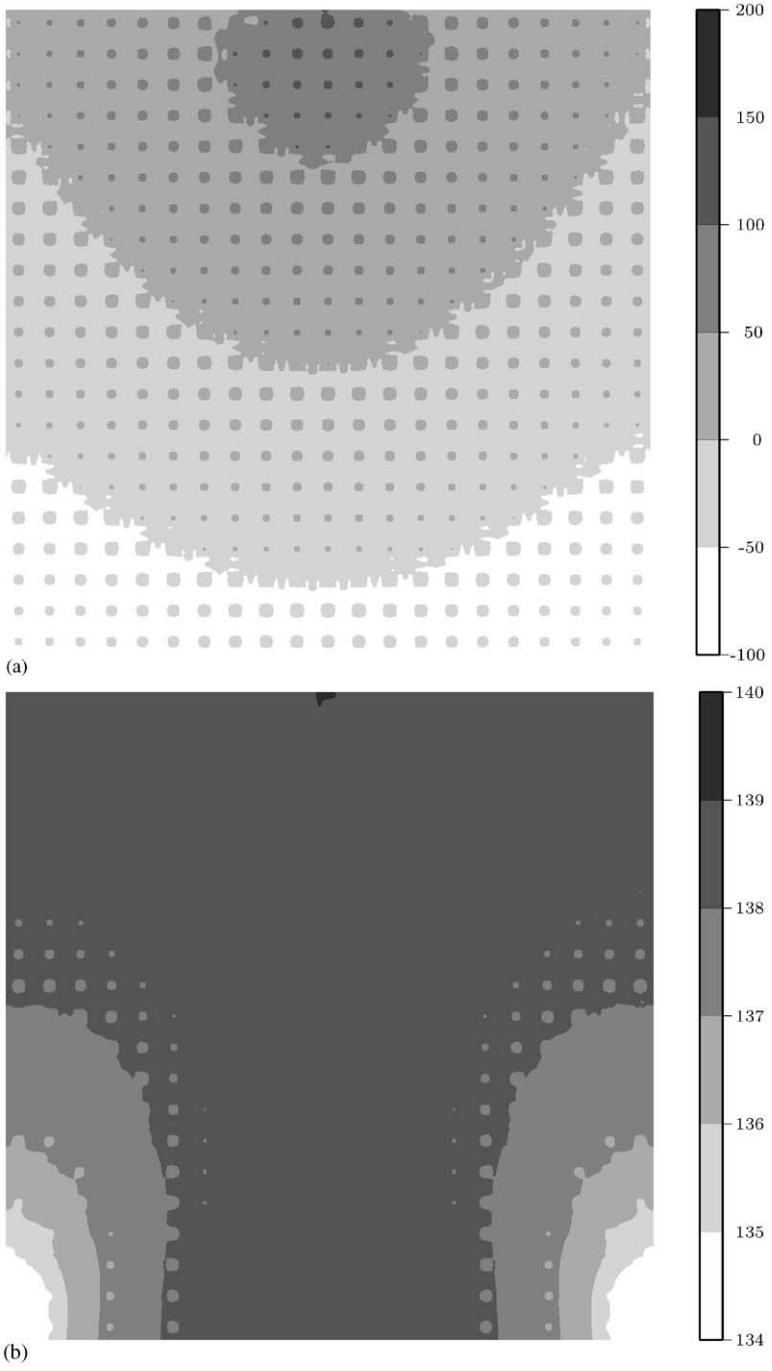

Fig. 13. (a) Contour plot of the structural response (in dB) for $\Omega = 1.34$ kHz, and (b) for $\Omega = 1.90$ kHz. Type 2 unit cells with $M_x = M_y = 21$.

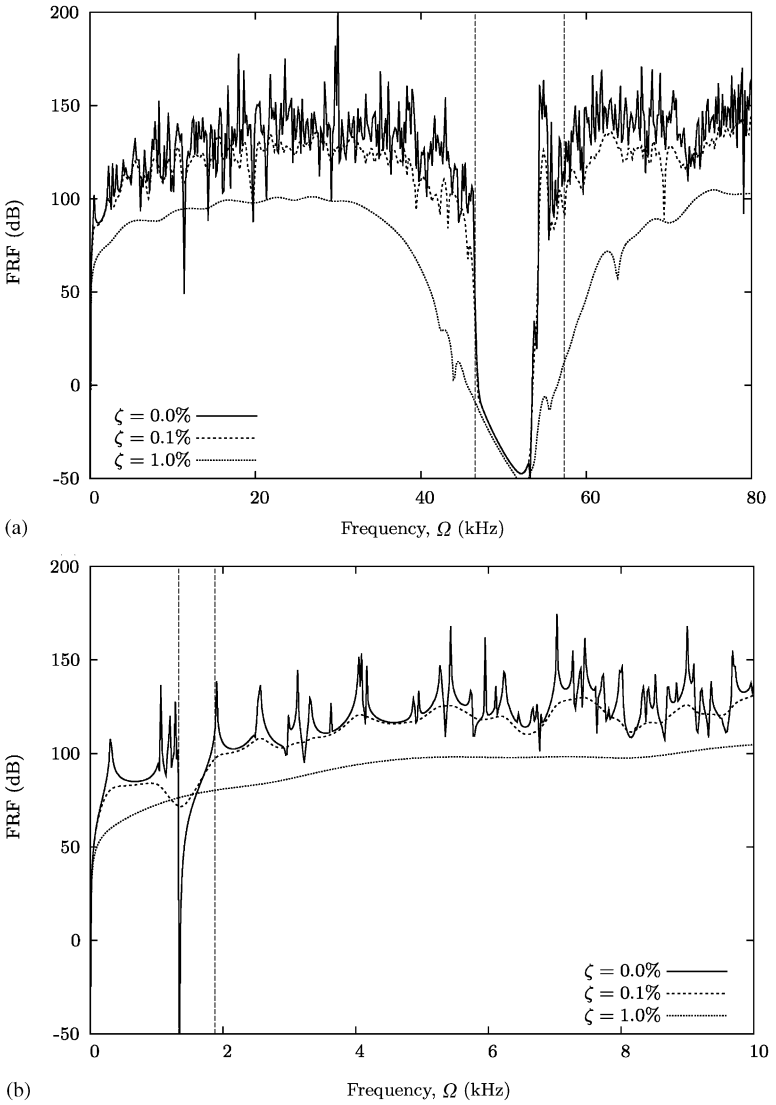

Fig. 14. The influence on the response of added viscous damping characterized by the actual to critical damping ratio ζ of the individual masses, (a) for type 1 unit cells, and (b) type 2 unit cells. In both figures $M_x = M_y = 21$.

periodic loading at certain frequency ranges. By introducing defects in the periodicity this effect can now be utilized to construct wave guides.

Type 1 unit cells are used in the following with $M_x = M_y = 21$. The defect is introduced by removing the inclusions from the unit cells in a path from the point of excitation in either a straight path to the bottom of the structure (point A) or in a 90° bent path to the side of the structure (point B).

Fig. 15a shows the response with a straight path of defects through the structure. It is seen that as for the perfect periodic structure the response in point B drops significantly in the band gap,

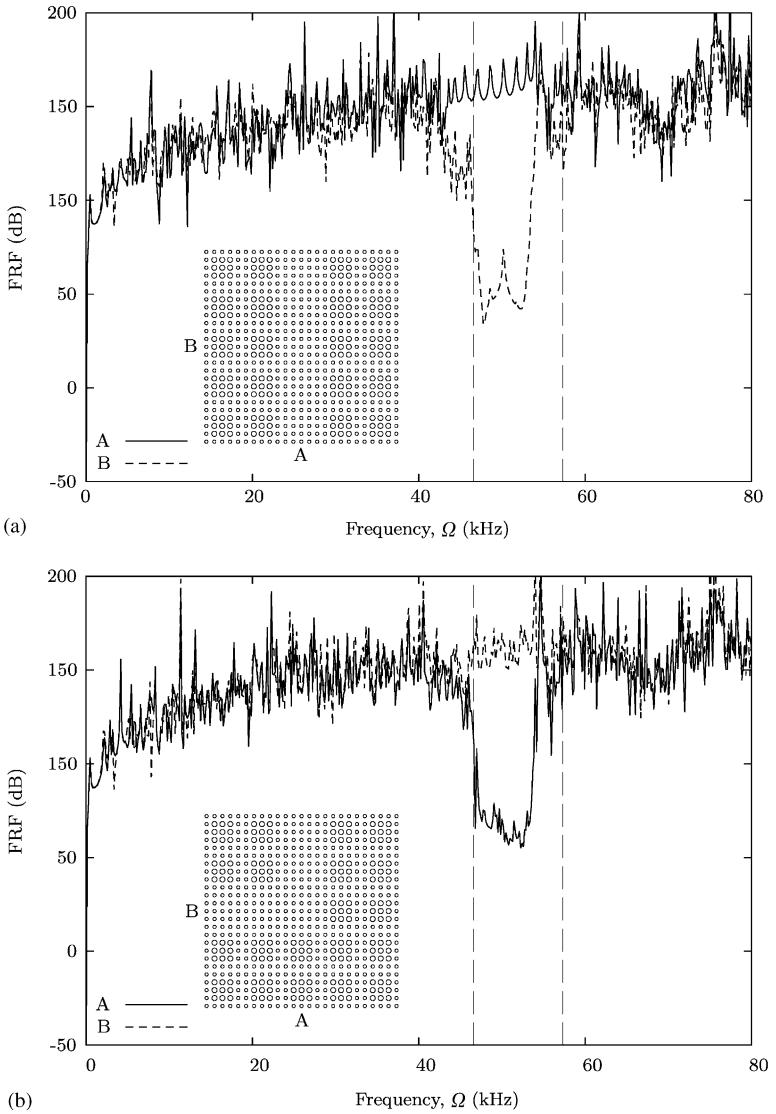

Fig. 15. The response in points A and B with a path of defects in the periodic structure for a the structure, (a) for vertical path, and (b) for a corner path. The insets show schematics of the paths. Type 1 unit cells with $M_x = M_y = 21$.

whereas in point A the response remains high indicating that the signal is now confined to the path. Fig. 15b shows the response for the bent path leading to point B. The response is now seen to be normalized in B inside the band gap, whereas in point A the response drops.

Contour plots of the response for the two lattice structures with paths are shown in Figs. 16a and b, respectively. The frequency of excitation for both figures is $\Omega = 52.1$ kHz, i.e., inside the band gap. The figure shows how the paths of defects in the periodic structures effectively isolates the vibrations to the path regions and thus "leads" the vibrations to the structural point A or B, whereas away from the paths the response drops rapidly with distance.

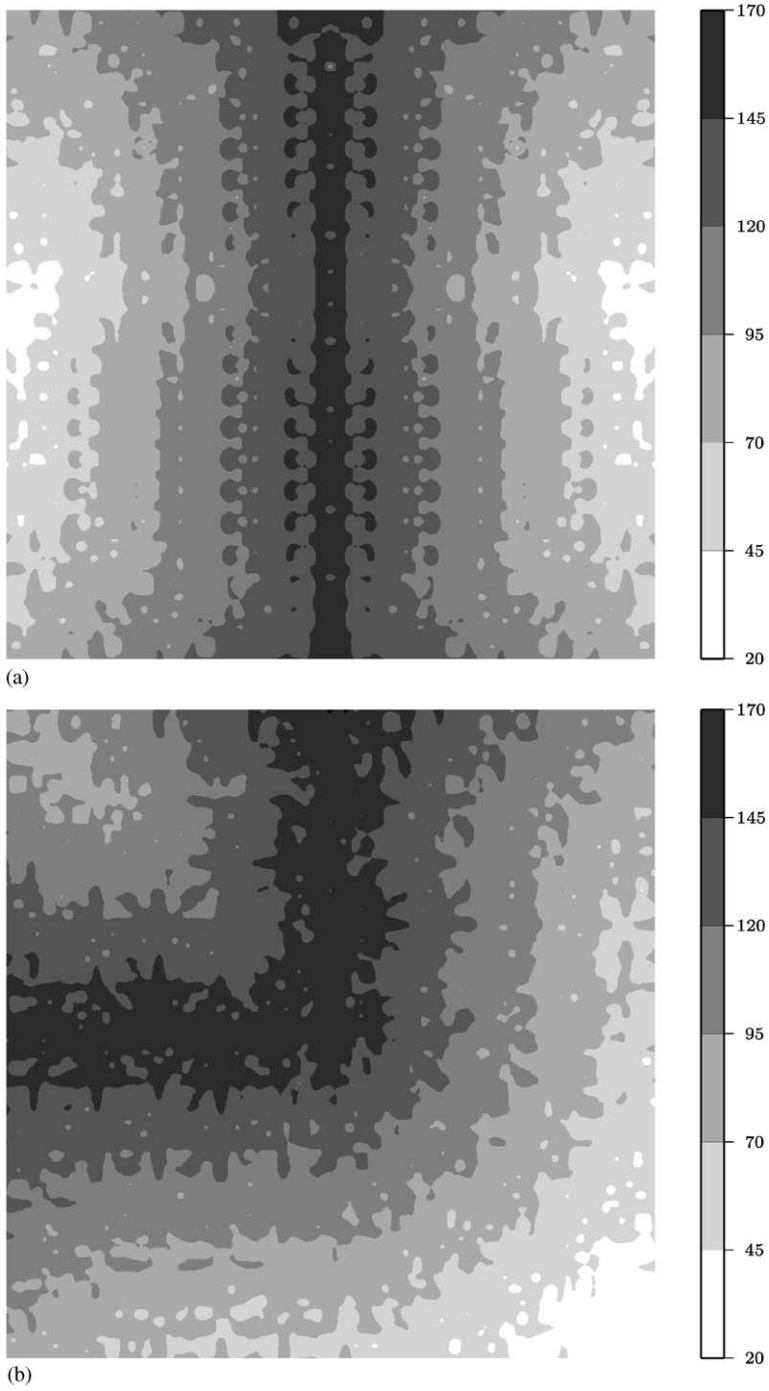

Fig. 16. Contour plot of the response for $\Omega = 52.1$ kHz, (a) for a vertical path of defects, and (b) for a corner path of defects. Type 1 unit cells with $M_x = M_y = 21$.

4. Conclusions

In order to use phononic band gap materials in mechanical structures that utilize the selective wave blocking abilities of these materials, the effects associated with the boundaries, damping, and imperfections need to be taken into account.

In this work the vibrational response of 1-D and 2-D mass–spring structures subjected to periodic loading has been investigated. The focus has been put on analyzing structures with a periodic micro-structure (unit cells) with gaps in the band structure for the corresponding infinite periodic lattice. Two examples were used to demonstrate the effect on the response of boundaries, viscous damping, and imperfections—a 1-D structure acting as a wave filter, and wave guiding in 2-D structures.

It was shown how the response in the band gap frequency range depends on the number of unit cells in the structure. In 1-D and for one of the two types of unit cells analyzed in 2-D, it was seen how the response in the band gap is insensitive to moderate amounts of viscous damping, whereas for the other 2-D unit cell analyzed, the band gap effect almost disappears with strong damping added. In the 1-D example it was shown also that the response in the band gap is insensitive to small imperfections in the periodic structure. It was demonstrated in both the 1-D and 2-D example, that the free boundaries cause local resonances that affect the response in the band gap. Two 2-D wave guides were analyzed, created by replacing the periodic structure with a homogeneous structure in a straight and a 90° bent path. It was shown how the vibrational response is confined to these paths in the band gap frequency ranges.

Further work deals with the formulation and solution of optimization problems that can be used to design of applications of phononic band gap materials and structures.

Acknowledgements

This work was supported by the Danish Research Council through the project "Phononic bandgap materials: Analysis and optimization of wavetransmission in periodic materials". The author would like to thank Jon Juel Thomsen, Ole Sigmund, and Martin P. Bendsøe for valuable comments and suggestions.

References

[1] J.D. Joannopoulos, R.D. Meade, J.N. Winn, Photonic Crystals, Molding the Flow of Light, Princeton University Press, Princeton, NJ, 1995.
[2] E. Yablonovitch, Photonic crystals: semiconductors of light, Scientific American 285 (2001) 34–41.
[3] Lord Rayleigh, On the maintenance of vibrations by forces of double frequency, and on the propagation of waves through a medium endowed with a periodic structure, Philosophical Magazine 24 (1887) 145–159.
[4] L. Brillouin, Wave Propagation in Periodic Structures, Dover Publications Inc, New York, 1953.
[5] C. Elachi, Waves in active and passive periodic structures: a review, Proceedings of the IEEE 64 (1976) 1666–1698.
[6] D.J. Mead, Wave propagation in continuous periodic structures: research contributions from Southampton, 1964–1995, Journal of Sound and Vibration 190 (1996) 495–524.
[7] S. Parmley, T. Zobrist, T. Clough, A. Perez-miller, M. Makela, R. Yu, Phononic band structure in a mass chain, Applied Physics Letters 67 (1995) 777–779.

[8] A. Diez, G. Kakarantzas, T.A. Birks, P.St.J. Russel, Acoustic stop-bands in periodically microtapered optical fibers, Applied Physics Letters 76 (2000) 3481–3483.
[9] D.J. Griffiths, C.A. Steinke, Waves in locally periodic media, American Journal of Physics 69 (2001) 137–154.
[10] M.M. Sigalas, E.N. Economou, Elastic and acoustic wave band structure, Journal of Sound and Vibration 158 (1992) 377–382.
[11] T. Suzuki, P.K.L. Yu, Complex elastic wave band structures in three-dimensional periodic elastic media, Journal of the Mechanics of Physics and Solids 46 (1998) 115–138.
[12] P. Langlet, A.-C. Hladky-hennion, J.-N. Decarpigny, Analysis of the propagation of plane acoustic waves in passive periodic materials using the finite element method, Journal of the Acoustical Society of America 98 (1995) 2792–2800.
[13] W. Axmann, P. Kuchment, An efficient finite element method for computing spectra of photonic and acoustic band-gap materials, Journal of Computational Physics 150 (1999) 468–481.
[14] Z. Liu, X. Zhang, Y. Mao, Y.Y. Zhu, Z. Yang, C.T. Chan, P. Sheng, Locally resonant sonic materials, Science 289 (2000) 1734–1736.
[15] J.O. Vasseur, P.A. Deymier, G. Frantziskonis, G. Hong, B. Djafari-rouhani, L. Dobrzynski, Experimental evidence for the existence of absolute acoustic band gaps in two-dimensional periodic composite media, Journal of Physics: Condensed Matter 10 (1998) 6051–6064.
[16] C.G. Poulton, A.B. Movchan, R.C. Mcphedran, N.A. Nicorovici, Y.A. Antipov, Eigenvalue problems for doubly periodic elastic structures and phononic band gaps, Proceedings of the Royal Society of London A 456 (2000) 2543–2559.
[17] M.S. Kushwaha, Classical band structure of periodic elastic composites, International Journal of Modern Physics 10 (1996) 977–1094.
[18] M. Torres, F.R. Montero de Espinosa, D. García-Pablos, N. García, Sonic band gaps in finite elastic media: surface states and localization phenomena in linear and point defects, Physical Review Letters 82 (1999) 3054–3057.
[19] I.E. Psarobas, N. Stefanou, A. Modinos, Phononic crystals with planar defects, Physical Review B 62 (2000) 5536–5540.
[20] O. Sigmund, Microstructural design of elastic band gap structures, in: G.D. Cheng, Y. Gu, S. Liu, Y. Wang (Eds.), Proceedings of the Second World Congress of Structural and Multidisciplinary Optimization, CD-rom, Liaoning Electronic Press, Dalian, China, 2001.
[21] O. Sigmund, J.S. Jensen, Topology optimization of phononic band gap materials and structures, Fifth World Congress on Computational Mechanics, Vienna, Austria, 2002, available at http://wccm.tuwien.ac.at.
[22] P.G. Martinsson, A.B. Movchan, Vibrations of lattice structures and phononic band gaps 56 (2003) 45–64.